High Energy Density Physics 23 (2017) 38–47

Contents lists available at ScienceDirect

High Energy Density Physics

journal homepage: www.elsevier.com/locate/hedp

Review of the 9th NLTE code comparison workshop

R. Piron[*,a], F. Gilleron[a], Y. Aglitskiy[1,b], H.-K. Chung[c], C.J. Fontes[d], S.B. Hansen[e], O. Marchuk[f], H.A. Scott[g], E. Stambulchik[h], Yu. Ralchenko[i]

[a] CEA, DAM, DIF, F-91297 Arpajon, France
[b] Leidos Inc, Reston, VA 20190, USA
[c] International Atomic Energy Agency, A-1400 Vienna, Austria
[d] Los Alamos National Laboratory, Los Alamos, NM 87545, USA
[e] Sandia National Laboratories, Albuquerque, NM 87185, USA
[f] Forschungszentrum Jülich, Inst Energie & Klimaforsch Plasmaphys, D-52425 Jülich, Germany
[g] Lawrence Livermore National Laboratory, Livermore, CA 94550, USA
[h] Faculty of Physics, Weizmann Institute of Science, Rehovot 7610001, Israel
[i] National Institute of Standards and Technology, Gaithersburg, MD 20899-8422, USA

ARTICLE INFO

Article History:
Received 23 February 2017
Accepted 23 February 2017
Available online 24 February 2017

Keywords:
Non-LTE plasmas
Collisional-radiative modeling
Population kinetics
Radiative properties
K-shell spectroscopy

ABSTRACT

We review the 9th NLTE code comparison workshop, which was held in the Jussieu campus, Paris, from November 30th to December 4th, 2015. This time, the workshop was mainly focused on a systematic investigation of iron NLTE steady-state kinetics and emissivity, over a broad range of temperature and density. Through these comparisons, topics such as modeling of the dielectronic processes, density effects or the effect of an external radiation field were addressed. The K-shell spectroscopy of iron plasmas was also addressed, notably through the interpretation of tokamak and laser experimental spectra.

1. Introduction

Various physical situations involve plasmas which cannot be described using the hypothesis of Local Thermodynamic Equilibrium (LTE). These include for instance the case of low-density plasmas which are not optically thick, or with a non-Planckian radiation drive, or the case of collisional plasmas with non-Maxwellian free-electron energy distributions. Consequently, Non-LTE (NLTE) plasma physics has a number of applications, among which are the design of indirect-drive laser-experiments [1], the problem of radiating impurities in tokamak discharges [2], the design of X-ray sources [3–5], the interpretation of plasma spectroscopy experiments [6], or the modeling of some astrophysical plasmas [7,8].

2. The NLTE workshops

The series of NLTE code comparison workshops [9–14] gathers, every two years, specialists of NLTE plasmas from all over the world. This workshop is dedicated to the investigation of the modeling of NLTE plasmas through the comparisons of results from different numerical codes. Current issues of NLTE plasma modeling are addressed and some experimental studies of NLTE plasmas are presented. The community of researchers who are involved in NLTE plasma modeling is rather small and this workshop gives them a unique opportunity to meet and discuss the latest improvements of their models and numerical codes. This workshop also allows newcomers to the field to quickly get an overview of the models that are implemented, methods that are used, and current main issues, which is not easy to figure out reading the literature.

The workshop proceeds as follows. Several months in advance, the scientific board sets a list of well-defined physical cases to study. The elements under study, electron densities, temperatures, and radiation fields are specified, as well as all supplementary information needed to precisely define the physical situations of interest. All of this information is specified in a call for submission, which also includes the format of the data that the contributors are expected to provide. People who wish to contribute to the workshop then run their codes, modifying them if necessary to treat the current cases of interest, and generate data that are collected in the workshop database. Shortly after the deadline for submissions, the database is made accessible to all contributors, especially to the case-leaders, who are charged with providing analyses and leading discussions on

* Corresponding author.
E-mail address: robin.piron@cea.fr (R. Piron).
[1] Present address: Naval Research Laboratory, Washington DC 20375, USA

http://dx.doi.org/10.1016/j.hedp.2017.02.009
1574-1818/

the cases. Some of the contributors then meet during 4–5 days in order to present the latest developments in their numerical codes and discuss the results that were submitted. Correction of errors and bugs is possible, as contributors may resubmit their data even after the meeting.

In order to prevent improper use of the results and to stimulate discussions, without hiding of the model and code caveats, a set of deontological rules was adopted:

- Only contributors can attend the workshop. Contribution can mean submission of results from a NLTE code or co-authorship of a code used to submit data. It can also mean the providing of experimental data used for comparisons. A few people may also be invited to give a talk on a specific topic.
- Only anonymized data from the workshop are publicly available, that is, data without attribution of results to specific codes. Contributors can only use the anonymized data in their publications, until they get an agreement of everyone involved. Of course they can freely use their own data.

The 9th edition of the NLTE workshop was held in the Jussieu campus, Paris, from November 30th to December 4th, 2015. Despite the tragic events that occurred in Paris on November 13th, 24 participants actually attended the meeting, which was the highest number ever reached. In addition to the case studies, this workshop included an invited talk by K. Fournier on the X-ray spectroscopy experiments on the National Ignition Facility, a special session on the use of the HULLAC [15] and FAC [16] detailed atomic physics packages, a few topical talks, and a posthumous tribute to V. G. Novikov.

In the past, the cases that were addressed in the workshops have included both rather low-Z elements, such as neon, and higher-Z elements, as for instance tungsten. This allowed the largest number of participants to contribute, since some detailed codes are not able to deal with high-Z elements. For this edition, the scientific board chose to limit the studies to one element: iron. Focusing the efforts of the participants on this sole element allowed us to perform a somewhat more systematic study. Moreover, iron is a mid-Z element, which still allows most people to contribute, at least for some of the density-temperature conditions. Finally, NLTE iron properties have a number of applications, ranging from astrophysics to the pollution of tokamak plasmas due to steel impurities. The 63 cases of interest for this systematic study are presented in Table 1. They span a broad range of temperature and density and include cases with a radiation drive, as well as with re-absorption over a given length. Among the new challenges of this edition was addressing the high-density regime, where all kinds of density effects can have an impact on the results.

In addition to these 63 regular iron cases, 4 experimental emission spectra were proposed for interpretation. One of these was from a tokamak experiment [40,41] and the three others were from laser experiments. The participants were asked to make a "best-fit" interpretation of the data using their own methodology and code, in order to grasp an idea of how diverse are the possible interpretations. Such exercises of interpretation were already per-

Table 1
Table of case definitions of the 9th NLTE workshop. The element under consideration is iron (Z=26). n_e, T_e are the free-electron density and temperature, respectively. T_R is the diluted Planckian radiation field temperature, dilution factor was 0.02. ℓ is the plasma length for the calculation of plasma re-absorption. λ denotes the wavelengths for the calculation of emissivity spectra.

n_e (cm^{-3})	10^{14}, 10^{19}, 10^{22}, 10^{24}
T_e (eV)	30, 60, 120, 200, 400, 700, 1000, 2000, 4000
T_R (eV)	0, 250 (only for $n_e = 10^{19}$)
ℓ (cm)	0, 0.1 (only for $n_e = 10^{19}$)
λ (Å;)	1.5 to 2 ($\Delta\lambda = 2.10^{-4}$), 10 to 18 ($\Delta\lambda = 2.10^{-3}$)

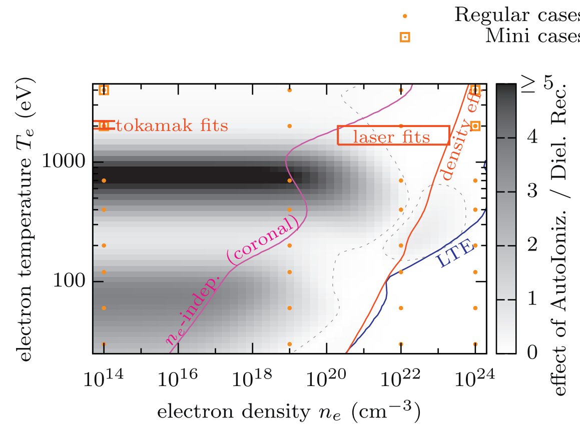

Fig. 1. (Color online) Plasma conditions of the NLTE-9 cases (without radiation drive). Dots correspond to the regular cases, squares correspond to the mini-test-cases. The temperature and density ranges of the best-fit interpretation of experimental spectra are also shown. The contours depict the regions corresponding to coronal equilibrium, LTE, non-negligible density effects, and non-negligible effects of dielectronic processes (dashed contour), respectively. These contours correspond to a 0.15 change of the mean ionization. The color map corresponds to the effect of dielectronic processes on the mean ionization. Calculations for this figure were done with the DEDALE code [26].

formed in previous workshops [6] and aim to evaluate how effectively the codes can be used to diagnose NLTE plasma experiments.

Finally, it was proposed to the participants to compute 4 particular cases ($n_e = 10^{14}, 10^{24}$ cm^{-3} and $T_e = 2000, 4000$ eV) using a minimal set of atomic levels, for which the level data and transition rates were given. The data for these "mini-test-cases" were generated using the FAC code.

Fig. 1 displays the NLTE-9 plasma conditions (for cases without any radiation drive) with the regions corresponding to

Table 2
Table of codes and contributors (alphabetical order, participants are in bold font, affiliation list in appendix).

Code	Refs	Contributors
ATLANTIS		M. Mendoza[k], J. Rubiano[j, k], R. Florido[j, k], J. Gil[j, k], R. Rodriguez[j, k], P. Martel[j, k], A. Benita[j], E. Minguez[j]
ATMED	[17]	**A. Benita**[j], E. Minguez[j], M. Mendoza[k], J. Rubiano[j, k], R. Florido[j, k], J. Gil[j, k], R. Rodriguez[j, k], P. Martel[j, k]
ATOMIC	[18,19]	J. Abdallah[d], J. Colgan[d], **C. J. Fontes**[d], H. L. Zhang[d]
AVERROES	[20–22]	C. Bowen[a], **F. Gilleron**[a] O. Peyrusse[l], **R. Piron**[a]
CANPS		Z. Wu[m]
CLOUDY	[23]	**G. Ferland**[n], **F. Guzman**[n]
CORH9	[24]	**M. Poirier**[o]
CRAC		**E. Stambulchik**[h]
CRETIN	[25]	**H.A. Scott**[g], **M. Hohensee**[g]
DEDALE	[26]	**F. Gilleron**[a], **R. Piron**[a]
DLAYZ	[27]	**J.M. Yuan**[p], **J.L. Zeng**[p]
FLYCHK	[28]	**H.-K. Chung**[c]
FOCH	[29]	M. Belkhiri[o] , **M. Poirier**[o]
HULLAC	[15,30]	**M. Busquet**[q] , **D. Gilles**[o]
JATOM	[31]	**A. Sasaki**[r]
NOHEL	in [10]	**A. Decoster**[a]
NOMAD	[32]	**Yu. Ralchenko**[i]
OPAZ		C. Blancard[a], Ph. Cossé[a], G. Faussurier[a]
SCRAM/SCSF	[33–35]	**S. B. Hansen**[e]
SCRIC	[36]	**F. de Gaufridy**[j]
SEMILLAC	[37,38]	**Y. Frank**[s]
SPECL		Z. Wu[m]
THERMOS	[39]	V. Novikov[t], A. Solomyannaya[t], **I. Vichev**[t]

different physical situations, such as coronal equilibrium, LTE, or the region in which density affects strongly the shell structure. As can be seen in this figure, the test cases cover all of these situations and a wide variety of modeling issues were addressed in this workshop.

Submissions from 53 modeling options of 23 different codes were gathered in the workshop database (see Table 2). The workshop is now mainly oriented towards the modeling of NLTE plasmas through the direct solution of the collisional-radiative (CR) set of equations (steady-state or time-dependent, see, for example, [42]), rather than through the use of effective temperatures. All the proposed modeling options however differ in a number of ways, as for instance their statistical treatment of the atomic energy levels, statistical completeness, method of choosing the set of levels, approximations for the cross-sections of the various processes, etc. They also differ as regards the numerical methods used for the computation of the transition rates or for the solution of the CR equation set.

Concerning the coarseness of the statistical treatment of the atomic levels, one can roughly distinguish a few categories:

- Average-Atom (AA) codes (ATMED, NOHEL, THERMOS, etc.)
- Configuration and/or Superconfiguration codes (AVERROES, some options of ATOMIC, etc.)
- Detailed Level Accounting codes, which are usually either based on FAC (CRAC, FOCH, NOMAD), HULLAC (CORH9, JATOM), Cowan's code [43] or RATS [18,19] (the latter two codes in connection with ATOMIC calculations)
- Hybrid codes, which mix different levels of details (SCRAM, some options of FLYCHK, CRETIN, DEDALE, etc.)

As regards the approach to the electronic structure of the atom, some codes implement a quantum calculation, some use a semiclassical approach [39] while some others use a semi-empirical Screened Hydrogenic Model [44,45]. With respect to the calculation of the cross-sections of the various atomic processes, some codes use approximate quantum calculations (such as the Born approximation [46] or distorted waves [47] for the collisional excitation cross-sections), whereas other codes use semi-empirical formulas (such as van Regemorter's [48]).

Such a variety in the complexity and degree of sophistication of the codes indeed reflects the diversity of their applications. Some codes are designed to perform the most precise calculations of the CR equilibrium (ATOMIC, AVERROES...). Other codes aim to perform rapid calculations, and are intended to be run inline in line-transfer or radiation-hydrodynamics simulations (NOHEL, FLYCHK, CRETIN, DEDALE, THERMOS...). The latter often use simplified models for the cross-sections of the various collisional and radiative transitions. Moreover, some codes are designed to diagnose plasma using high-resolution spectroscopy whereas others are designed to give an estimate of broad-band radiative properties.

3. Discussion of results

3.1. $n_e = 10^{14}$ and 10^{19} cm^{-3} cases

Such low-density plasmas may be relevant to tokamak physics, or to some astrophysical applications such as the solar corona. The lowest-density case, namely $n_e = 10^{14}$ cm^{-3}, without any radiation drive, is typical of the so-called low-density coronal limit (see, for instance, [49],§5-5). In the coronal limit, the excitation channels are dominated by collisional excitation (CE) as the radiation field is negligible, and the de-excitation channels are dominated by spontaneous emission (SE) as the electron density is low. Recombination is dominated by radiative recombination (RR) and dielectronic recombination (DR). Among the dominant ionization channels is collisional

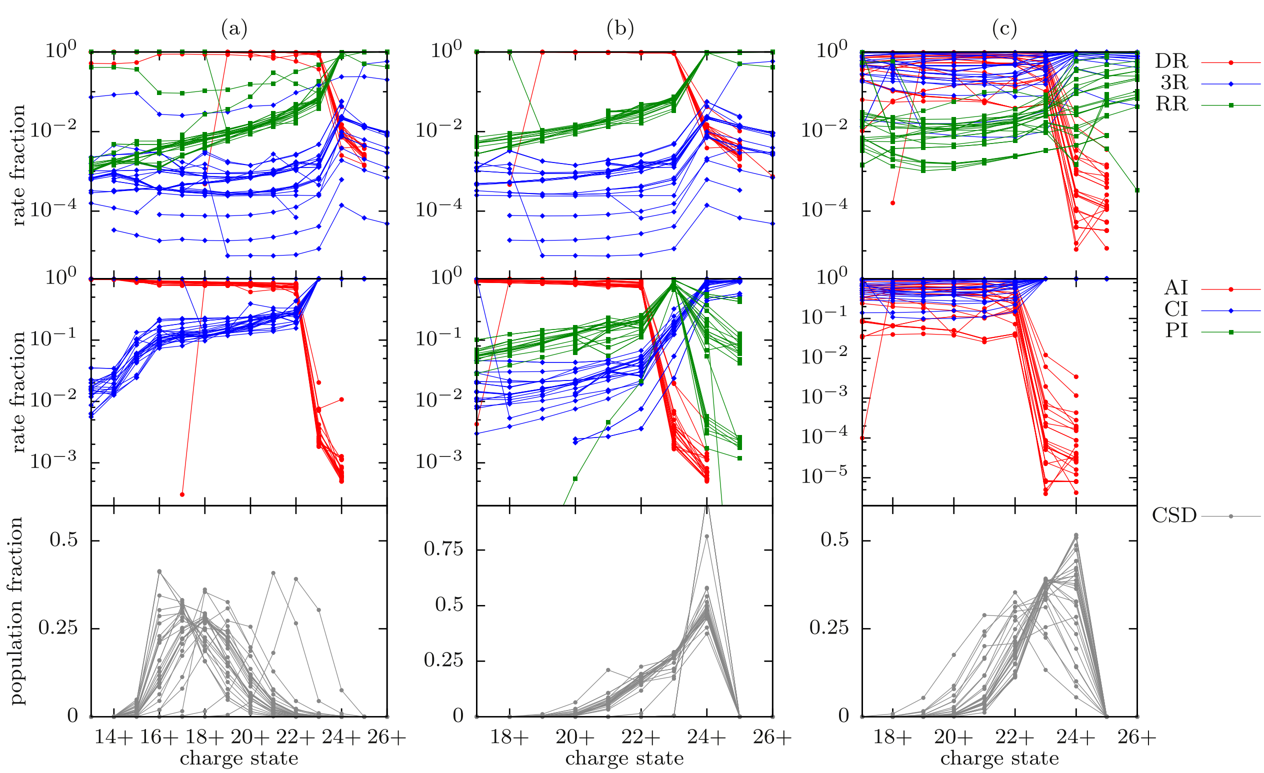

Fig. 2. (Color online) Charge state distributions (CSDs) and fractional ionization and recombination rates, from the various NLTE codes for three different $T_e = 700$ eV cases: (a) $n_e = 10^{19}$ cm^{-3} without radiation drive, (b) $n_e = 10^{19}$ cm^{-3} with radiation drive, and (c) $n_e = 10^{22}$ cm^{-3}. CI denotes collisional ionization. AI denotes autoionization, which is of course zero for bare and H-like ions. PI denotes photoionization, which is non-zero only in the (b) case. RR, 3R and DR denote radiative, 3-body, and dielectronic recombinations, respectively.

ionization (CI), but as soon as complex ions are involved, the contribution of excitation-autoionization (EA) channels cannot be neglected (see [50,51]). These are mostly collisional excitations to autoionizing levels from the ground states and in the present cases, they often dominate. In case of a low-density coronal plasma, the charge state distribution (CSD) only depends on the electron temperature, and not on the electron density. Indeed, most of the codes give mean ionizations at $n_e = 10^{19}$ cm^{-3} that differ from that at $n_e = 10^{14}$ cm^{-3} only at low temperatures (mean ionizations differ by less than 5% for $T_e \geq 200$ eV). For instance, it is shown in Fig. 2a, that at $n_e = 10^{19}$ cm^{-3}, $T_e = 700$ eV, the CR equilibrium still mainly consists of a balance between EA and CI on one hand, and DR and RR on the other hand.

Mean ionizations from the various NLTE codes are displayed as a function of the free-electron temperature in Figs. 3 and 4 for the $n_e = 10^{14}$ and 10^{19} cm^{-3} cases, respectively. Significant disagreement among codes is observed in both cases, except at temperatures that correspond to closed-shell configurations (i.e. Ne-like and He-like). The false impression of agreement within a denser array of curves is due to the presence of multiple submissions from a few codes (included for didactic purposes). In the past, such disagreements at low density were studied for argon cases [14]. By simply switching off the EA/DR accounting, they were shown to be mostly related to the modeling of EA/DR channels. Here, the highest outlier corresponds to a modeling option where all EA/DR transitions are disregarded. Among the lowest outliers are the AA codes based on the Albritton–Wilson [52] approach to the EA/DR. Agreement around ions with closed-shell ground configurations may stem from the closing of the Coster-Kronig channels (i.e. $\Delta n = 0$ AI/DR, [53]) in closed-shell configurations (see [14]). Indeed, the accounting for Coster–Kronig channels is among the main differences between models. In some models, especially those in which levels are binned into Layzer complexes, these transitions are often simply disregarded. In the case of charge states above Li-like, the AI/DR total rate drops down (see Fig. 2). Ultimately, AI from H-like to bare ion and its inverse are of course not possible. This also tends to improve agreement when CSDs are centered on the He-like ion.

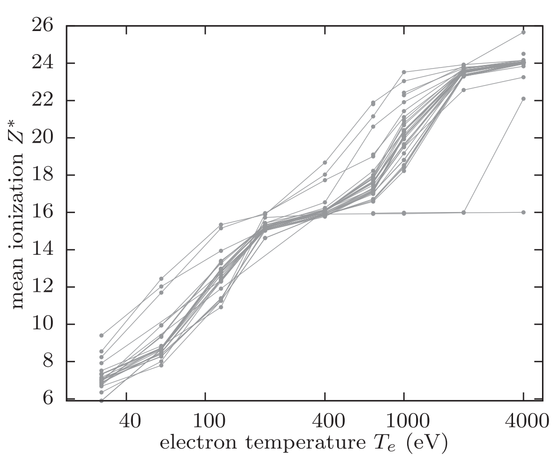

Fig. 3. Mean ionization as a function of free-electron temperature, from the various NLTE codes for the $n_e = 10^{14}$ cm^{-3} cases.

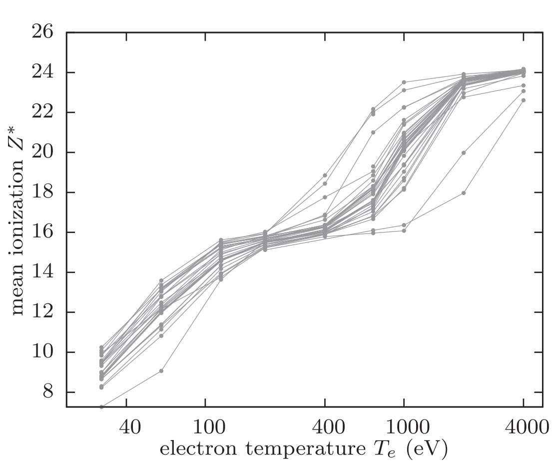

Fig. 4. Mean ionization as a function of free-electron temperature, from the various NLTE codes for the $n_e = 10^{19}$ cm^{-3} cases, without a radiation drive.

When the external radiation drive is considered (Planckian at $T_R = 250$ eV, with a dilution factor of 0.02), the rise of photoionization (PI) and photoexcitation (PE) to autoionizing levels results in larger mean ionization (see Fig. 2b). Mean ionizations from the various NLTE codes are displayed as a function of the free-electron temperature in Fig. 5 for the 10^{19} cm^{-3} case with external radiation drive. Most of the codes yield CSDs that are centered on Be-like to He-like ions, over the whole temperature range. As can be seen in Fig. 2b, for Li-like to bare ions, the balance proceeds from a competition between CI and PI on one hand and RR on the other. Be-like and more complex ions remain mainly driven by EA/DR. The Li-like ground state has an ionization threshold around 2 keV, which is much closer to the frequency range of the radiation drive than the threshold of the He-like (around 8–9 keV). This may explain why ionization from Li- to He-like mainly occurs through PI. Again, the agreement between codes gradually improves as the He-like charge state is reached.

Concerning the case with re-absorption, the prescribed re-absorption length of 1 *mm* was actually too short to observe significant effects. We therefore do not consider a separate analysis for this case.

Finally, in both low density cases, the disagreement in radiative power losses (RPLs) can typically reach a factor of 10 (excluding the contributions that had obvious units issues). As an example, Fig. 6 displays the RPLs from the various codes as functions of the electron temperature, in the 10^{19} cm^{-3} case (without radiation drive). There, one can see the effect of the shell structure on the RPL. Moreover, it is worth noting that the disagreements in RPL can be largest at temperatures that correspond to closed-shell configurations, where the disagreements on the mean ionization are minimal.

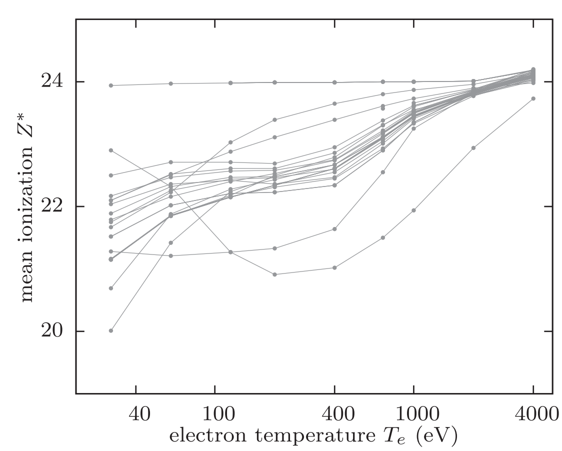

Fig. 5. Mean ionization as a function of free-electron temperature, from the various NLTE codes for the $n_e = 10^{19}$ cm^{-3} cases, with a diluted Planckian external radiation drive (temperature $T_R = 250$ eV and dilution factor of 0.02). Some outliers that do not seem to have considered the right problem were removed from this comparison.

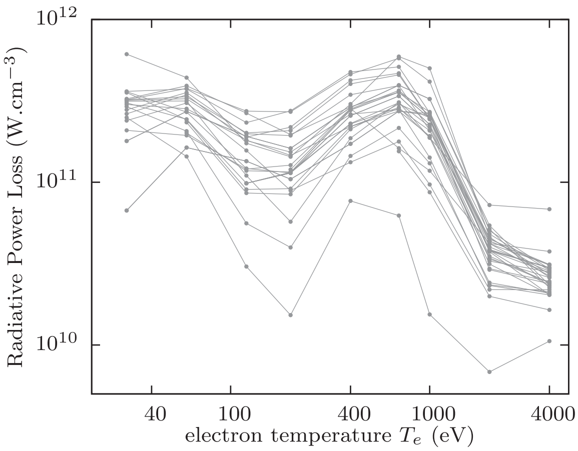

Fig. 6. Radiative power loss (RPL) as a function of free-electron temperature, from the various NLTE codes for the $n_e = 10^{19}$ cm^{-3} cases, without a radiation drive.

3.2. $n_e = 10^{22}$ cm^{-3} case

This case includes density/temperature conditions that are typical for NLTE radiation hydrodynamics applications to laser-created plasmas. As can be seen in Fig. 7, the agreement in the mean ionization is better than for the lowest two densities. This can be explained by the collisional processes, which compete with AI/DR for complex ions, and even dominate in some models (see Fig. 2c). For He-like to bare ions, 3-body recombination (3R) competes with the RR, which dominates at lower densities.

Not only the mean ionizations, but also the RPLs, are in rather good agreement. These agree within a factor of 2, which is typically the best agreement we can reach for an LTE calculation (see next section). Moreover, the agreement in RPL seems qualitatively independent of the closed-shell effects, that is, RPLs from the various codes seem to roughly differ by multiplicative constants.

In order to go a little further into the detail of the radiative properties, Fig. 8 shows the K− and L−shell spectra of the $T_e = 2$ keV and 200 eV cases, respectively. In both of these cases, we obtain rather good agreement among the codes in the mean ionization (see Fig. 7). The case of $T_e = 200$ eV is quite close to LTE, whereas the $T_e = 2$ keV case is relatively insensitive to the AI/DR (see Fig. 1). The calculated strengths from the various codes for the K_α feature at $T_e = 2$ keV, as well as for the 2−3 features at $T_e = 200$ eV are within a factor of 2, which seems consistent with the level of agreement in the RPL.

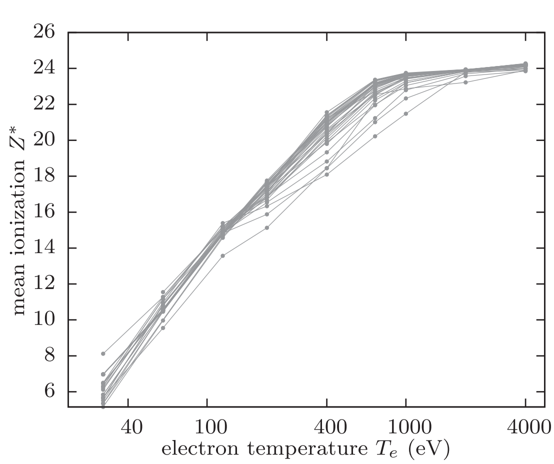

Fig. 7. Mean ionization as a function of free-electron temperature, from the various NLTE codes for the $n_e = 10^{22}$ cm^{-3} cases.

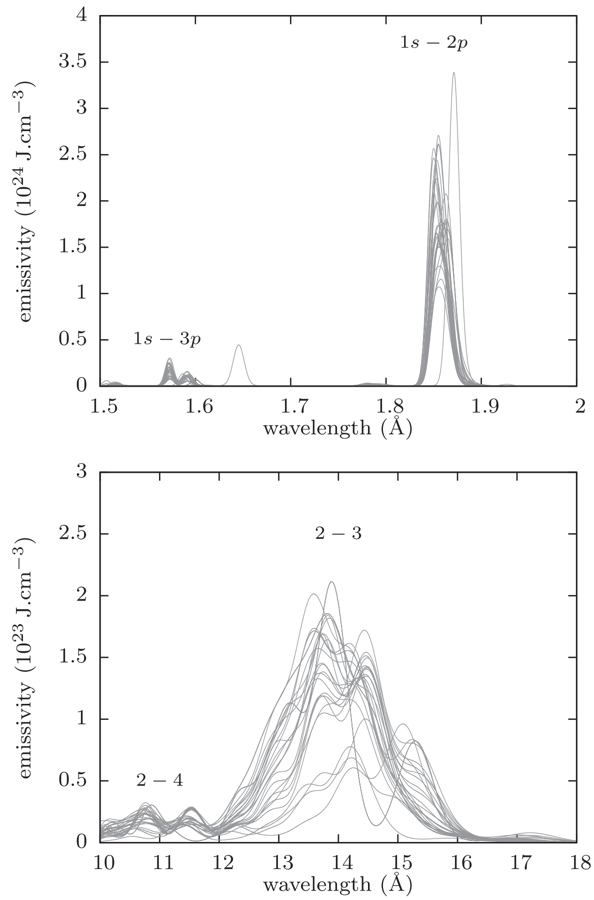

Fig. 8. Top: K-shell spectrum of the $n_e = 10^{22}$ cm^{-3}, $T_e = 2$ keV case (close to He-like). An arbitrary 20 eV broadening has been applied for the sake of comparison between the different codes. Bottom: L-shell spectrum of the $n_e = 10^{22}$ cm^{-3}, $T_e = 200$ eV case (close to Ne-like). An arbitrary 15 eV broadening has been applied for the sake of comparison between the different codes.

Finally, it is worth noting the large spread of total statistical weights among the codes, spanning over 9 decades, even when one disregards the outliers (see Fig. 9). This may indicate that statistical completeness is not crucially required in order to model the plasma CR equilibrium in this regime. Here, a limited number of well-chosen

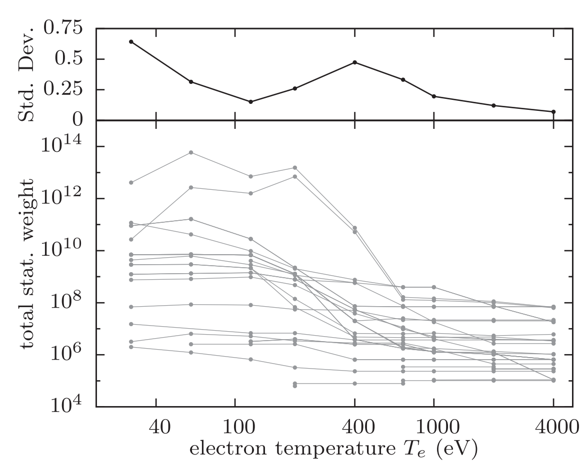

Fig. 9. Cases of intermediate density $n_e = 10^{22}$ cm^{-3}. Total statistical weights from a subset of the NLTE codes, among which a quantitative agreement is found. The standard deviation on Z^* among the results is displayed on top. It remains below one charge state over the whole temperature range.

levels seem enough to capture the channels that are relevant to the CR equilibrium over a broad range of temperatures.

3.3. $n_e = 10^{24}$ cm^{-3} case

This high density case is relevant to all applications that involve near-solid-density plasmas, such as Inertial Confinement Fusion, or stellar astrophysics. At such high densities, all kinds of density effects are to be expected, including massive 3-body recombination, electron and ion Stark broadening of lines, merging of lines into unresolved arrays, and pressure ionization.

The impact of high density on the electronic structure of atoms in a plasma is a long-standing issue of plasma physics, and remains an open question. This issue is usually addressed in the context of plasmas in thermodynamic equilibrium, for which ever more sophisticated models are proposed. Indeed, dense plasmas are most often strongly dominated by collisional processes with thermalized free electrons, which results in LTE. However, an intermediate regime exists, in which plasmas are not fully in LTE and yet the density has an impact on the electronic structure. Several physical pictures are candidates for describing dense plasmas. Among them is the notion of continuum lowering [54,55], and various self-consistent models of atoms inspired by solid state physics [39,56–61]. These pictures often produce contradictory results and it is hard to identify which one constitutes a realistic description of dense plasmas, if one of them does. Recently, experiments have attempted to tackle the high-density regime using X-ray Free Electron Lasers [62], or laser-induced shock compression [63].

Due to the theoretical and practical complexity of some approaches, only a few of them are actually used in NLTE modeling and one often resorts to the simplest heuristic approaches. Among the codes, the impact of density on the atomic shell structure is accounted for in quite different ways, ranging from rather involved models such as the quasizone model [39] to purely heuristic degeneracy reduction [26,64], or even a simple rule of thumb for the limitation of the maximum principal quantum number.

Fig. 10 shows the mean ionization curves from the various NLTE codes. This figure also shows the mean ionization stemming from a non-relativistic version of Liberman's Inferno model [58], using two different definitions of the mean ionization (see Fig. 10 caption). Despite its known thermodynamic inconsistency issue in the low-temperature/high-density regime [61], this equilibrium model is often used in equation-of-state calculations and includes a rather involved accounting for the density effects, inspired by solid-state physics.

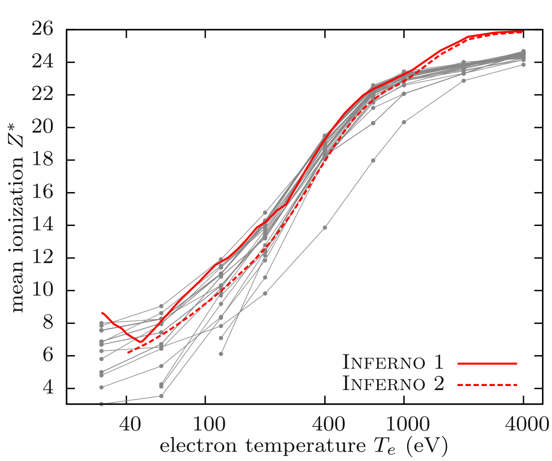

Fig. 10. (Color online) Mean ionization as a function of free-electron temperature for the $n_e = 10^{24}$ cm^{-3} cases, from the various NLTE codes and from the Inferno model. Inferno 1 denotes the curve obtained using the definition: $Z^* = Z - N_{\text{bound}}$, where N_{bound} is the total population of bound states. Inferno 2 denotes the curve obtained using the definition: $Z^* = \frac{\sqrt{2}T^{3/2}}{\pi^2 n_i} I_{1/2}\left(\frac{\mu}{T}\right)$, where $I_{1/2}$ is the Fermi integral of order 1/2, and where μ is the chemical potential, T is the temperature, and n_i is the ion density, all in atomic units.

Unfortunately, mean ionization is not identically defined in every model, and one should be careful when comparing mean ionizations from models that are not based on the same physical picture of an atom in a plasma. In particular, in quantum models, the definition of mean ionization does not always rely on an observable of quantum mechanics.

In this workshop, most of the NLTE models are based on the picture of an ideal gas mixture of point-like ions and free electrons. The internal electronic structure of ions is that of free ions, possibly corrected to account for the impact of density. In the limit of thermodynamic equilibrium, all the species tend to be in chemical equilibrium, i.e. the model tends to a Saha model. In these models, the mean ionization is the ratio of the population of free electrons to the total population of ions, which are well-defined quantities.

By contrast, in the Inferno model, no distinction among electrons is in principle relevant. Using definition 1, displaced continuum electrons in the vicinity of nuclei are categorized as free electrons, and the mean ionization jumps each time a populated bound state disappears. In this respect, the present mean ionization could be viewed as an upper bound for the mean ionization of Saha-like models. Definition 2 corresponds to only considering as free, those electrons that are not polarized by the ions. Qualitatively, we can then expect the mean ionization of the Saha-like models that account for density effects to be located somewhere in between the two curves.

At the lowest temperatures, typically below 200 eV, the radiative processes are negligible for both de-excitation and recombination. Processes that are in detailed balance strongly dominate and it can be confirmed with the level populations that the plasma is in LTE, for which the level populations are independent of the rates. However, a large spread among the results is observed. This is due to differences in accounting for density effects on the shell structure, which are strong in these cases. Indeed, these temperatures correspond to matter densities above solid density. It is worth noting that among the lowest outliers are all the models that do not account for any impact of density on the electronic structure. In these models, the effect of 3R results in low mean ionizations at high densities.

At higher temperatures, agreement among the NLTE codes improves. This agreement among NLTE codes can be explained by the fact that the plasma is still in LTE, whereas the density effects on the shell structure decrease. As the mean ionization increases, the remaining bound electrons are statistically localized on core shells, which are less impacted by density. On the other hand, the higher the mean ionization, the lower the ion density at a given electron density. The Wigner–Seitz radius then increases with temperature (at 1 keV, the matter density is about half the solid density).

At temperatures above 1 keV, the agreement among NLTE codes holds but disagreement with the Inferno curves is observed. The disagreement with Inferno is due to a gradual departure from LTE.

At temperatures between 400 eV and 1 keV, the plasma is near LTE and density is not dramatically affecting the shell structure. The calculated RPLs in these cases typically agree within a factor of 2. This gives an idea of the level of agreement that is achieved for the RPL, independently of density effects and NLTE modeling issues. At the lowest temperatures, for which density affects the shell structure, disagreement typically reaches a factor of 10 in the RPL.

3.4. Tokamak spectrum

The experimental tokamak spectrum proposed for "best-fit" interpretation is shown in Fig. 11. It was obtained on the TORE SUPRA facility and was provided by O. Marchuk [40,41]. The plasma

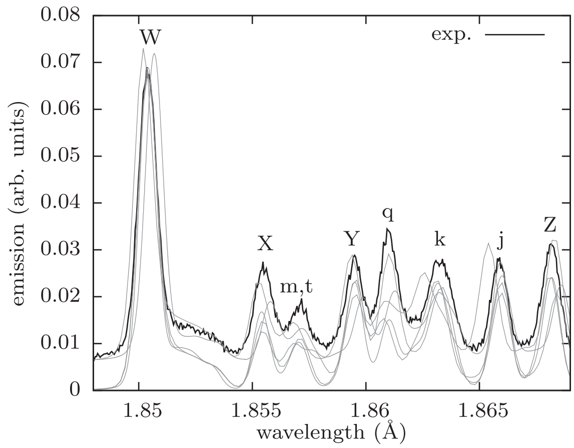

Fig. 11. Tokamak experimental spectrum and "best-fit" interpretations from the NLTE codes. For sake of readability, only codes performing a detailed accounting of the main lines are shown. The spectroscopic notation of [65] is used.

density conditions ($n_e \sim 10^{13}$–10^{14} cm^{-3}) are very close to coronal and the results are density-independent. The interpretation therefore only consists of determining the plasma temperature.

In the spectrum (see Fig. 11), one can identify E2, M1, and M2 lines due to radiative transitions from metastable fine-structure levels. The shoulder on the red-wing of the W line (i.e. He$_\alpha$ resonance line) is composed of its Li-like satellites of the type $1s^2n\ell$–$1s2pn\ell$, with $n \geq 3$. In order to correctly describe this spectrum, it is crucial to include in the kinetic model a detailed level accounting, at least for some well-chosen energy levels. The interpretation of the spectrum then mainly relies on obtaining a balance between He-like and Li-like charge states that yields the correct strength ratios between the W,X,Y,Z lines and the m,t,q,k,j satellites.

Eight codes participated in this interpretation. One of them used a fraction of non-Maxwellian free-electrons. The temperatures inferred from the spectrum using the various codes range from 1.9 keV to 2.2 keV. These temperatures may seem to be in rather good agreement. However, considering the CSDs (see Fig. 12), one can see that this temperature spread of about 15% corresponds to a factor of 3 spread in the He-like to Li-like population ratios. As can be seen in Fig. 11, these quite different results however lead to rather similar spectra. Of course disagreements are mostly in the line strengths. Slight disagreements are also observed in line positions since some codes use tabulated line positions from the NIST database whereas others rely on FAC calculations, and the spectral range is so narrow that even the precision of the conversion from energies to wavelengths can slightly affect the positions.

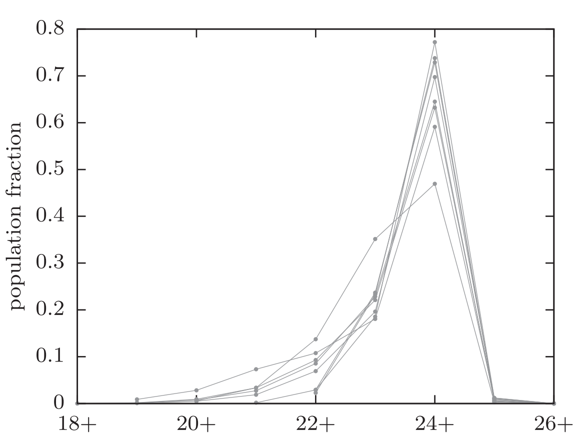

Fig. 12. Charge state distributions (CSDs) corresponding to the "best-fit" interpretations of the tokamak spectrum.

3.5. Laser spectra

The laser spectra proposed for "best-fit" interpretation are shown in Fig. 13. These were obtained on the Nike laser facility and were provided by Y. Aglitskiy. They are published here for the first time. Among the main features of the spectra, one can identify the He$_\alpha$ resonance and intercombination lines (W and Y), as well as Li-like satellites of the He$_\alpha$ resonance line. The He-like levels which produce the X and Z lines of the tokamak spectrum are much less populated in the present case. The collisional de-excitation channels are indeed much larger than the E1-forbidden radiative decays, since the free-electron density is much larger.

Eight contributions were submitted for these cases. The temperatures inferred from spectrum 1 using the various codes range from 1.4 keV to 2.0 keV. For spectrum 2, they range from 1.0 keV to 1.5 keV and, for spectrum 3, they range from 1.4 keV to 1.7 keV. We then have deviations of about 20% in T_e among the interpretations.

On the other hand, the inferred electron densities span two orders of magnitude. The line widths in these spectra are mainly related to macroscopic plasma effects as well as spectrometer resolution rather than solely to the Stark broadening and therefore do not provide precise information about the electron density of the plasma. Thus, the estimate of the plasma density, just as the estimate

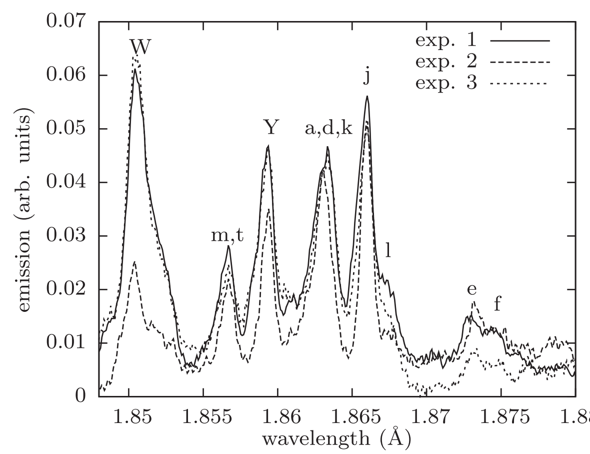

Fig. 13. Laser experimental spectra. The spectroscopic notation of [65] is used.

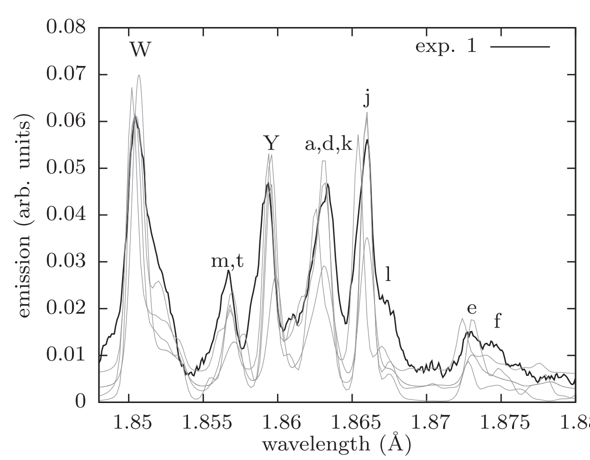

Fig. 14. Laser experimental spectrum 1 and "best-fit" interpretations from the NLTE codes. For sake of readability, only codes performing a detailed accounting of the main lines are shown. The spectroscopic notation of [65] is used.

of the temperature, relies on the study of line-intensity ratios. In the regime of interest for these experiments, the CSD is in large part driven by CI and 3R (Li-like to H-like ions). The effects of electron density and temperature on CI/3R can partially compensate each other, if one increases both the electron density and temperature. Similar results may then be obtained from higher-density/higher-temperature pairs as well as for lower-density/lower-temperature pairs. However, with such a small number of contributions, no clear correlation between the inferred temperature and density is found.

Again, it can be checked in Fig. 14 that the different interpretations, with such different densities, lead to quite similar spectra.

3.6. Mini-test-cases

The mini-test-cases are four chosen cases from Table 1, namely the $n_e = 10^{14}; 10^{24}$ cm^{-3}, $T_e = 2; 4$ keV cases, for which the set of energy levels and atomic physics data were given. The levels are the 22 fine-structure levels of the He-like and H-like configurations $1s^2$, $1s2\ell$, $2\ell2\ell'$, $1s$, 2ℓ, as well as the bare ion level. The data included labels, parities, degeneracies and energies of the levels, as well as the rates of resonant processes and tabulated values of cross-sections for non-resonant processes. All of these data were computed by E. Stambulchik using cFAC [66], a modified version of the FAC code [16]. Starting from these data, the participants were asked to calculate the CR equilibrium case using their own methods of computing the rates of non-resonant processes, of accounting for density effects, of solving the CR set of equations, and of calculating the emissivity. Contributions of eight codes were gathered for these mini-test-cases. Some of the participants had in fact used their own atomic data obtained either from HULLAC or from FAC. In the latter case, the data were quite close, but still non-identical, to those that were given.

In all of these mini-test-cases, the considered charge states range from He-like to bare ion. Moreover, the given set only includes autoionizing levels with electrons on the L shell (He-like $2\ell2\ell'$ levels). For these reasons, dielectronic processes play a relatively minor role in the ionization balance, which mostly proceeds from a competition between CI and RR. The spread among the mean ionizations reaches 0.15, in the $n_e = 10^{24}$ cm^{-3}, $T_e = 4$ keV case. As can been seen in Fig. 15, this moderate spread however corresponds to a significant disagreement in the CSD. This disagreement may be related to differences in the rates of non-resonant processes (RR, CE, CI and their inverse processes). The calculation of these rates requires integration over energy of the product of a particle flux and a cross-section. In the framework of the mini-test-case, the values of the cross-sections are provided at some sampling points. In order to perform

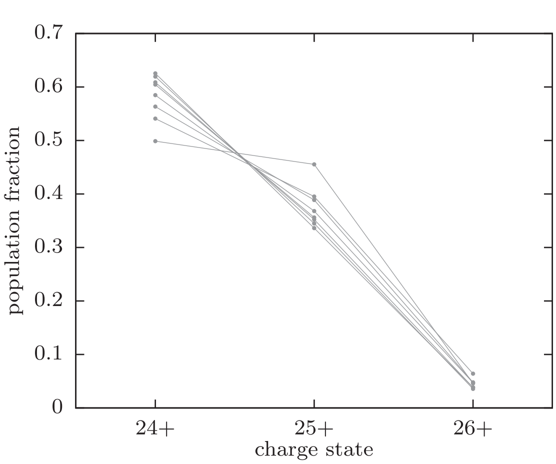

Fig. 15. Charge state distributions (CSDs) for the $n_e = 10^{24}$ cm^{-3}, $T_e = 4$ keV mini-test-case.

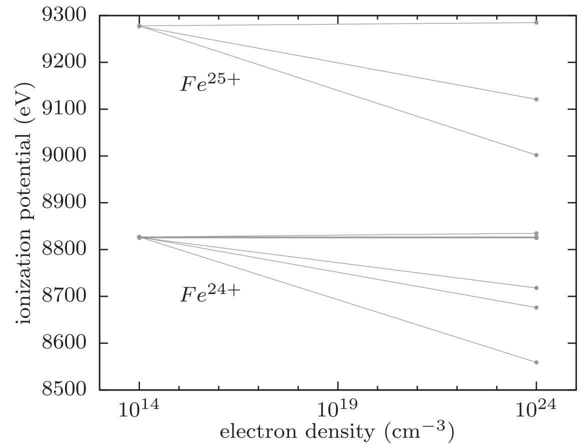

Fig. 16. He-like and H-like ionization potentials for the $T_e = 2$ keV mini-test-cases.

the integration, one can either integrate between the sampling points using some interpolation scheme, or fit some analytical formula on the sampling points and then use an analytical form of the integral. In general, performing the integral up to infinity is necessary and one needs to extrapolate, using an asymptotic form of the cross-section. The method of performing the numerical integration, and the choice of a particular asymptotic form of the cross-section, can significantly affect the rate evaluations. The fact that the disagreement is more pronounced at the higher density and temperature may indicate that it is mostly due to collisional processes. At high densities, the accounting for density effects on the shell structure (see Fig. 16) may also have a significant impact on the level energies and thus on the populations, through detailed balance.

Even in a case for which a good agreement is found in the kinetics, such as $n_e = 10^{14}$ cm^{-3}, $T_e = 2$ keV (mean ionization spread of 0.02, very similar CSDs), the RPLs disagree significantly. The spread among Bremsstrahlung contributions to the RPL is about 30%, which is likely due to the use of different Gaunt factors.

4. Conclusions

The series of NLTE workshops offers a kind of realistic picture of science, without hiding its share of scientific errors, theoretical deficiencies, technical bugs, or naive questions. Of course, the global methodology of these workshops has both advantages and drawbacks.

Among the drawbacks is some normalizing tendency. Participants tend to develop similar modeling options (use of ionization potential depression, decreasing number of AA codes in favor of configuration or superconfiguration codes, etc.) or to use similar tools (generalized use of FAC). Even the format of the submission data can strongly influence the participants, since it is not equally suited to all models. It should be noted, however, that even when using similar atomic physics data, some spread among the results remains, leading to deeper investigations of the underlying methods and their impact on the results.

This kind of workshop remains essential to people involved in NLTE plasmas modeling. It allows them to test their models and numerical codes, which is particularly important in a field lacking in reference databases and benchmark experiments. Although it remains mostly limited to "code-to-code" comparisons, some actual issues of NLTE plasma modeling can be addressed in this workshop.

This workshop is also a periodic event that stimulates the development of numerical tools, asking slightly different questions each time. Due to the diversity of the applications of NLTE plasmas physics, this workshop is finally an opportunity for distinct research communities to meet, including those of laser-created plasmas, X-ray sources, tokamak physics, and astrophysical plasmas.

The rate of progress over the last couple of workshops may seem to have diminished. This probably indicates that progress is occurring slowly on some known issues such as balance between accuracy and statistical completeness, or better accounting for the EA/DR channels (even in the coronal limit). On the other hand, there remain a lot of relevant issues, which have not been addressed in these workshops. Among these are for instance the effect of non-Maxwellian free-electron distributions, systematic studies of external radiation drive, time-dependent CR modeling, and the impact of uncertainties in the atomic data on the results of CR models.

We also note that practically all considered cases of the present edition actually produced relevant comparisons. Focusing our efforts on only one element in order to perform a systematic study gave us more useful points of comparison for the analyses. The interpretation of experimental spectra gathered a greater number of contributions than in previous editions. During this edition, we also addressed some topics more deeply than in the previous ones, such as density effects in NLTE plasmas, which for sure need to be even further explored. A new comparison method was also introduced: the use of “mini-test-cases”, which allowed us to investigate the impact of cross-section interpolation methods and asymptotic forms on the CR modeling.

Acknowledgements

The organizers of the NLTE-9 workshop acknowledge financial support from the CEA, DAM, DIF and technical support from the NIST. They would also like to thank the UTES, Université Pierre et Marie Curie, which have provided local support as subcontracters for the meeting room and related IT. Thanks are also due to all of the participants for their valuable contributions and the fruitful discussions that occurred during the workshop.

The work of CJF was performed under the auspices of the United States Department of Energy under contract DE–AC52–06NA25396.

The work of HAS was performed under the auspices of the United States Department of Energy under contract DE–AC52–07NA27344.

Appendix. List of the contributor affiliations

Supplementary list of affiliations:

[j]Departamento de Física, Universidad de Las Palmas de Gran Canaria, 35017 Las Palmas de Gran Canaria, Spain.

[k]Instituto de Fusion Nuclear, Universidad Politecnica de Madrid, 28006 Madrid, Spain.

[l]Aix-Marseille Université, Lab. PIIM, UMR 7345, F-13397 Marseille, France.

[m]Institute of Applied Physics and Computational Mathematics, Beijing 100088, China.

[n]Physics Department, University of Kentucky, Lexington, KY 40506, USA.

[o]Laboratoire “Interactions, Dynamiques et Lasers”, UMR 9222, CEA-CNRS-Université Paris-Saclay, Centre d’Études de Saclay, F-91191 Gif-sur-Yvette Cedex, France.

[p]Department of Physics, College of Science, National University of Defense Technology, Changsha Hunan 410073, China.

[q]ARTEP Inc, Ellicott City, MD 20375, USA.

[r]Quantum Beam Science Directorate, Japan Atomic Energy Agency, 8-1 Umemidai, Kizugawa-shi, Kyoto 619-0215, Japan.

[s]Soreq Research Center, Yavne 81800, Israel.

[t]Keldysh Institute of Applied Mathematics, Russian Academy of Sciences, Moscow, Russia.

References

[1] M.D. Rosen, H.A. Scott, D.E. Hinkel, E.A. Williams, D.A. Callahan, R.P.J. Town, L. Divol, P.A. Michel, W.L. Kruer, L.J. Suter, R.A. London, J.A. Harte, G.B. Zimmerman, The role of a detailed configuration accounting (DCA) atomic physics package in explaining the energy balance in ignition-scale hohlraum, High Energy Density Phys. 7 (2011) 180–190.

[2] R.E.H. Clark, D. Reiter (Eds.), Nuclear Fusion Research – Understanding Plasma-Surface Interactions, Springer-Verlag, 2005.

[3] M. Primout, D. Babonneau, L. Jacquet, F. Gilleron, O. Peyrusse, K.B. Fournier, R. Marrs, M.J. May, R.F. Heeter, R.J. Wallace, Characterization of a hybrid target multi-keV x-ray source by a multi-parameter statistical analysis of titanium K-shell emission, High Energy Density Phys. 18 (2016) 55–66.

[4] A. Dasgupta, R.W. Clark, J.L. Giuliani, N.D. Ouart, B. Jones, D.J. Ampleford, S.B. Hansen, K-α Emission spectroscopic analysis from a Cu Z-pinch, High Energy Density Phys. 9 (2013) 347–353.

[5] M. Poirier, T. Blenski, F. de Gaufridy de Dortan, F. Gilleron, Modeling of EUV emission from xenon and tin plasma sources for nanolithography, J. Quant. Spectrosc. Radiat. Transf. 99 (2006) 482–492.

[6] S.B. Hansen, G.S.J. Armstrong, S. Bastiani-Ceccotti, C. Bowen, H.-K. Chung, J. Colgan, F. de Dortan, C.J. Fontes, F. Gilleron, J.-R. Marquès, R. Piron, O. Peyrusse, M. Poirier, Y. Ralchenko, A. Sasaki, E. Stambulchik, F. Thais, Testing the reliability of non-LTE spectroscopic models for complex ions, High Energy Density Phys. 9 (2013) 523–527.

[7] G.J. Ferland, Quantitative spectroscopy of photoionized clouds, Annu. Rev. Astron. Astrophys. 41 (2003) 517–554.

[8] C.J. Fontes, K.A. Eriksen, J. Colgan, H.L. Zhang, J.P. Hughes, Spectral modeling of supernova remnants, High Energy Density Phys. 10 (2014) 43–46.

[9] R.W. Lee, J.K. Nash, Y. Ralchenko, Review of the NLTE kinetics code workshop, J. Quant. Spectrosc. Radiat. Transfer 58 (1997) 737–742.

[10] C. Bowen, A. Decoster, C.J. Fontes, K.B. Fournier, O. Peyrusse, Y.V. Ralchenko, Review of the NLTE emissivities code comparison virtual workshop, J. Quant. Spectrosc. Radiat. Transfer 81 (2003) 71—84.

[11] C. Bowen, R.W. Lee, Y.V. Ralchenko, Comparing plasma population kinetics codes: review of the NLTE-3 kinetics workshop, J. Quant. Spectrosc. Radiat. Transfer 99 (2006) 102–119.

[12] J.G. Rubiano, R. Florido, C. Bowen, R.W. Lee, Y.V. Ralchenko, Review of the 4th NLTE code comparison workshop, High Energy Density Phys. 3 (2007) 225–232.

[13] C.J. Fontes, J. Abdallah Jr, C. Bowen, R.W. Lee, Y. Ralchenko, Review of the NLTE-5 kinetics workshop, High Energy Density Phys. 5 (2009) 15–22.

[14] H.-K. Chung, C. Bowen, C.J. Fontes, S.B. Hansen, Y. Ralchenko, Comparison and analysis of collisional-radiative models at the NLTE-7 workshop, High Energy Density Phys. 9 (2013) 645–652.

[15] A. Bar-Shalom, M. Klapisch, J. Oreg, HULLAC, an integrated computer package for atomic processes in plasmas, J. Quant. Spectrosc. Radiat. Transfer 71 (2001) 169–188.

[16] M.F. Gu, The flexible atomic code, Can. J. Phys. 86 (2008) 675–689.

[17] A.J. Benita, E. Mínguez, M.A. Mendoza, J.G. Rubiano, J.M. Gil, R. Rodríguez, P. Martel, Collisional radiative average atom code based on a relativistic screened hydrogenic model, High Energy Density Phys. 14 (2015) 18–29.

[18] C.J. Fontes, H.L. Zhang, J. Abdallah, R.E.H. Clark, D.P. Kilcrease, J. Colgan, R.T. Cunningham, P. Hakel, N.H. Magee, M.E. Sherrill, The Los Alamos suite of relativistic atomic physics codes, J. Phys. B 48 (2015) 144014.

[19] D.H. Sampson, H.L. Zhang, C.J. Fontes, A fully relativistic approach for calculating atomic data for highly charged ions, Phys. Rep. 477 (2009) 111–214.

[20] O. Peyrusse, Atomic configuration averages and non-local thermodynamical equilibrium plasma spectroscopy calculations, J. Phys. B 32 (1999) 683–700.

[21] O. Peyrusse, A superconfiguration model for broadband spectroscopy of non-LTE plasmas, J. Phys. B 33 (2000) 4303–4321.

[22] O. Peyrusse, On the superconfiguration approach to model NLTE plasma emission, J. Quant. Spectrosc. Radiat. Transfer 71 (2001) 571–579.

[23] G.J. Ferland, R.L. Porter, P.A.M. van Hoof, R.J.R. Williams, N.P. Abel, M.L. Lykins, G. Shaw, W.J. Henney, P.C. Stancil, The 2013 release of Cloudy, Rev. Mex. Astron. Astrofis. 49 (2013) 137–163.

[24] M. Poirier, F. de Gaufridy de Dortan, A comparison between detailed and configuration-averaged collisional-radiative codes applied to nonlocal thermal equilibrium plasmas, J. App. Phys. 101 (2007) 063308.

[25] H.A. Scott, S.B. Hansen, Advances in NLTE modeling for integrated simulations, High Energy Density Phys. 6 (2010) 39–47.

[26] F. Gilleron, R. Piron, The fast non-LTE code DEDALE, High Energy Density Phys. 17 (2015) 219–230.

[27] C. Gao, J. Zeng, Y. Li, F. Jin, J. Yuan, Versatile code DLAYZ for investigating population kinetics and radiative properties of plasmas in non-local thermodynamic equilibrium, High Energy Density Phys. 9 (2013) 583–593.

[28] H.-K. Chung, M.H. Chen, W.L. Morgan, Y. Ralchenko, R.W. Lee, FLYCHK: generalized population kinetics and spectral model for rapid spectroscopic analysis for all elements, High Energy Density Phys. 1 (2005) 3–12.

[29] M. Belkhiri, Plasma out of Thermodynamical Equilibrium : Influence of the Plasma Environment on Atomic Structure and Collisional Cross Sections, 2014 Ph.D. thesis.

[30] M. Busquet, A. Bar-Shalom, M. Klapisch, J. Oreg, An improved version of the HULLAC code, J. Phys. IV France 133 (2006) 973–975.

[31] A. Sasaki, Construction of a collisional radiative model of complex multiple charged ions for mid- to high-Z elements, High Energy Density Phys. 9 (2013) 325–335.

[32] Y. Ralchenko, Y. Maron, Accelerated recombination due to resonant deexcitation of metastable states, J. Quant. Spectrosc. Radiat. Transfer 71 (2001) 609–621.
[33] S.B. Hansen, J. Bauche, C. Bauche-Arnoult, M.F. Gu, Hybrid atomic models for spectroscopic plasma diagnostics, High Energy Density Phys. 3 (2007) 109–114.
[34] S.B. Hansen, Configuration interaction in statistically complete hybrid-structure atomic models, Can. J. Phys. 89 (2011) 633.
[35] S.B. Hansen, J. Bauche, C. Bauche-Arnoult, Superconfiguration widths and their effects on atomic models, High Energy Density Phys. 7 (2011) 27.
[36] F. de Gaufridy de Dortan, SCRIC - Un code pour calculer l'absorption et l'émission détaillées de plasmas hors équilibre inhomogènes et étendus, Technical Report CEA-R-6115, 2006.
[37] Y. Frank, E. Louzon, P. Mandelbaum, Z. Henis, SEMILLAC: a new hybrid atomic model of hot dense plasmas, High Energy Density Phys. 9 (2013) 594–600.
[38] Y. Frank, P. Mandelbaum, Z. Henis, SEMILLAC II: a new model for spectral behavior of hot plasmas, High Energy Density Phys. 12 (2014) 27–34.
[39] A.F. Nikiforov, V.G. Novikov, V.B. Uvarov, Quantum-Statistical Models of Hot Dense Matter, Birkhauser, 2005.
[40] O. Marchuk, Modeling of He-like Spectra Measured at the Tokamaks TEXTOR and TORE SUPRA, 2004 Ph.D. thesis.
[41] O. Marchuk, G. Bertschinger, C. Fenzi-Bonizec, B. Schunke, M. Mattioli, A. Whiteford, N.R. Badnell, Impurity transport studies in TORE SUPRA with He-like spectroscopy, 32nd EPS Conference on Plasma Phys. ECA, 29C, 2005, pp. P–2.025.
[42] Y. Ralchenko (Ed.), Modern Methods in Collisional-Radiative Modeling of Plasmas, Springer International Publishing Switzerland, 2016.
[43] R.D. Cowan, The Theory of Atomic Structure and Spectra, University of California Press, 1981.
[44] R.M. More, Electronic energy-levels in dense plasmas, J. Quant. Spectrosc. Radiat. Transf. 27 (1982) 345–357.
[45] F. Perrot, Fast calculation of electronic structure in plasmas. The screened hydrogenic model with l-splitting, J. Phys. 12 (49) (1988) C7–285−C7−289.
[46] I.I. Sobel'man, L.A. Vainshtein, E.A. Yukov, Excitation of Atoms and Broadening of Spectral Lines, 2nd, Springer-Verlag, 1995.
[47] H.L. Zhang, D.H. Sampson, A.K. Mohanty, Fully relativistic and quasirelativistic distorted-wave methods for calculating collision strengths for highly charged ions, Phys. Rev. A 40 (1989) 616–632.
[48] H. van Regemorter, Rate of collisional excitation in stellar atmospheres, Astrophys. J. 136 (1962) 906–915.
[49] D. Mihalas, Stellar Atmospheres, W. H. Freeman and Co., 1978.
[50] C. Jordan, The ionization equilibrium of elements between carbon and nickel, Mon. Not. R. Astr. Soc. 142 (1969) 501–521.
[51] V.L. Jacobs, J. Davis, P.C. Kepple, M. Blaha, The influence of autoionization accompanied by excitation on dielectronic recombination and ionization equilibrium, Astrophys. J. 211 (1977) 605–616.
[52] J.R. Albritton, B.G. Wilson, Non-LTE ionization and energy balance in high-Z laser plasmas including two-Electron transitions, Phys. Rev. Lett. 83 (1999) 1594–1597.
[53] D. Coster, R.d.L. Kronig, A new type of Auger effect and its influence on the X-ray spectrum, Physica 2 (1935) 13–24.
[54] G. Ecker, W. Kröll, Lowering of the ionization energy for a plasma in thermodynamic equilibrium, Phys. Fluids 6 (1963) 62–69.
[55] J.C. Stewart, K.D. Pyatt, Lowering of ionization potentials in plasmas, Astrophys. J. 144 (1966) 1203–1211.
[56] R.P. Feynman, N. Metropolis, E. Teller, Equation of state of elements based on the generalized Fermi-Thomas theory, Phys. Rev. 75 (10) (1949) 1561–1573.
[57] B.F. Rozsnyai, Relativistic Hartree-Fock-Slater calculations for arbitrary temperature and matter density, Phys. Rev. A 5 (3) (1972) 1137–1149.
[58] D.A. Liberman, Self-consistent field model for condensed matter, Phys. Rev. B 20 (12) (1979) 4981–4989.
[59] B.J.B. Crowley, Average-atom quantum-statistical cell model for hot plasma in local thermodynamic equilibrium over a wide range of densities, Phys. Rev. A 41 (1990) 2179–2191.
[60] T. Blenski, B. Cichocki, Variational theory of average-atom and superconfigurations in quantum plasmas, Phys. Rev. E 75 (2007) 056402.
[61] R. Piron, T. Blenski, Variational-average-atom-in-quantum-plasmas (VAAQP) code and virial theorem: equation-of-state and shock-Hugoniot calculations for warm dense Al, Fe, Cu, and Pb, Phys. Rev. E 83 (2011) 026403.
[62] O. Ciricosta, S.M. Vinko, H.-K. Chung, B.-I. Cho, C.R.D. Brown, T. Burian, J. Chalupsky, K. Engelhorn, R.W. Falcone, C. Graves, V. Hajkova, A. Higginbotham, L. Juha, J. Krzywinski, H.J. Lee, M. Messerschmidt, C.D. Murphy, Y. Ping, D.S. Rackstraw, A. Scherz, W. Schlotter, S. Toleikis, J.J. Turner, L. Vysin, T. Wang, B. Wu, U. Zastrau, D. Zhu, R.W. Lee, P. Heimann, B. Nagler, J.S. Wark, Direct measurments of the ionization potential depression in a dense plasma, Phys. Rev. Lett. 109 (2012) 065002.
[63] D.J. Hoarty, P. Allan, S.F. James, C.R.D. Brown, L.M.R. Hobbs, M.P. Hill, J.W.O. Harris, J. Morton, M.G. Brookes, R. Shepherd, J. Dunn, H. Chen, E. Von Marley, P. Beiersdorfer, H.-K. Chung, R.W. Lee, G. Brown, J. Emig, Observations of the effect of ionization-potential depression in hot dense plasma, Phys. Rev. Lett. 110 (2013) 265003.
[64] G.B. Zimmerman, R.M. More, Pressure ionization in laser-fusion target simulation, J. Quant. Spectrosc. Radiat. Transf. 23 (1980) 517–522.
[65] A.H. Gabriel, Dielectronic satellite spectra for highly-charged helium-like ion lines, Mon. Not. R. Astr. Soc. 160 (1972) 99–119.
[66] E. Stambulchik, cFAC website: http://github.com/fnevgeny/cfac/.